JGR Atmospheres

RESEARCH ARTICLE
10.1029/2025JD044492

Special Collection:
Chemistry and Climate Impacts of the Asian Summer Monsoon

Comparison of Daily Ozonesonde Measurements and Chemical Reanalyses Over South Korea Based on 2021 Pre-ACCLIP Data: An Ozone Intrusion Case

Hyungyu Kang[1,2], Su-Bin Oh[1], Ja-Ho Koo[3], Sang Seo Park[4], Anne M. Thompson[5], Ryan M. Stauffer[5], Debra E. Kollonige[5], Won-Jin Lee[6], Jinsoo Park[6], Laura L. Pan[7], Shawn B. Honomichl[7], Sanghyun An[1], and Joowan Kim[1,2]

[1]Department of Atmospheric Science, Kongju National University, Gongju, South Korea, [2]Particle Pollution Research and Management Center, Gongju, Republic of Korea, [3]Department of Atmospheric Sciences, Yonsei University, Seoul, South Korea, [4]Department of Civil, Urban, Earth, and Environmental Engineering, Ulsan National Institute of Science & Technology (UNIST), Ulsan, South Korea, [5]Atmospheric Chemistry and Dynamics Laboratory, NASA/GSFC, Greenbelt, MD, USA, [6]National Institute of Environmental Research, Incheon, South Korea, [7]Atmospheric Chemistry Observations and Modeling Laboratory, NCAR, Boulder, CO, USA

Key Points:

- Daily ozonesonde measurements captured an intense synoptic-scale ozone enhancement event in the upper troposphere–lower stratosphere (UTLS) over Korea in August 2021
- The enhanced ozone event was directly linked to anticyclonic wave breaking on the eastern periphery of the Asia summer monsoon anticyclone
- Modern-Era Retrospective Analysis for Research and Applications, Version 2 and European Centre for Medium-Range Weather Forecasts (ECMWF) Atmospheric Composition Reanalysis 4 well reproduced synoptic ozone patterns but exhibited substantial differences in the UTLS and near the surface

Supporting Information:

Supporting Information may be found in the online version of this article.

Correspondence to:
J. Kim,
joowan.k@gmail.com

Citation:
Kang, H., Oh, S.-B., Koo, J.-H., Park, S. S., Thompson, A. M., Stauffer, R. M., et al. (2025). Comparison of daily ozonesonde measurements and chemical reanalyses over South Korea based on 2021 Pre-ACCLIP data: An ozone intrusion case. *Journal of Geophysical Research: Atmospheres*, *130*, e2025JD044492. https://doi.org/10.1029/2025JD044492

Received 2 JUN 2025
Accepted 15 NOV 2025

Abstract This study investigates an ozone intrusion event observed during the Pre-Asian Summer Monsoon Chemical and Climate Impact Project in August 2021, using 26 consecutive daily ozonesonde measurements over South Korea. A pronounced enhancement in total column ozone was observed between 17 and 19 August, which can be largely attributed to an ozone intrusion in the upper troposphere–lower stratosphere (UTLS), accounting for approximately 60% of the increase. The upper tropospheric circulation patterns demonstrate a clear signature of anticyclonic Rossby wave breaking (AWB) on the northeastern edge of the Asian summer monsoon anticyclone, aligned with the summertime jet stream. This AWB, accompanied by a cut-off low and tropopause folding, facilitated downward transport of stratospheric ozone into the upper troposphere. In addition, the ozone variability is investigated in two chemical reanalysis data sets: Modern-Era Retrospective Analysis for Research and Applications, Version 2 (MERRA-2) and European Centre for Medium-Range Weather Forecasts (ECMWF) Atmospheric Composition Reanalysis 4 (EAC4). MERRA-2 and EAC4 capture the ozone intrusion event with relevant synoptic-scale circulation patterns and ozone variability. However, discrepancies of ozone data in the chemical reanalyses were found in vertical ozone structures and persistence in the troposphere. MERRA-2 better represented the secondary ozone peak in the UTLS but underestimated lower-tropospheric ozone. In contrast, EAC4 showed a systematic positive bias particularly in the stratosphere and near the surface. Continued integration of temporally high-resolution ozone measurements is beneficial for understanding synoptic-scale ozone variability and evaluating emerging chemical reanalyses.

Plain Language Summary This study used 26 daily balloon-borne ozone sensors launched in South Korea during August 2021. These observations captured a rapid ozone increase caused by stratospheric air intrusion into the upper troposphere. Analysis reveals that the increase in ozone was directly induced by wave breaking and mixing processes between the troposphere and the stratosphere near the Asia summer monsoon anticyclone. We used these measurements to evaluate two widely used chemical reanalyses (Modern-Era Retrospective Analysis for Research and Applications, Version 2 (MERRA-2) and European Centre for Medium-Range Weather Forecasts (ECMWF) Atmospheric Composition Reanalysis 4 (EAC4)) ozone. The reanalyses captured the ozone enhancement event qualitatively, however they showed notable quantitative differences vertically. The EAC4 tended to overestimate ozone in the stratosphere and near the surface. The MERRA-2 also overestimated ozone in the stratosphere, but underestimated ozone closer to the surface. These differences are likely related to how satellite data is used and how the atmospheric chemistry is handled in the reanalyses. Our results emphasize that daily ozonesonde measurements are useful for evaluation of the synoptic variabilities in the chemical reanalyses.

1. Introduction

The upper troposphere–lower stratosphere (UTLS) is a dynamically complex region in which stratospheric and tropospheric air masses frequently interact, exerting influence on global atmospheric composition, radiative forcing, and climate variability (Gettelman et al., 2011; Manney et al., 2011; Riese et al., 2012; Tao et al., 2018).

This transition zone is characterized by sharp gradients in temperature and chemical composition, making it a critical interface for the exchange and transport of trace gases, notably ozone and water vapor (Fueglistaler et al., 2005; Gettelman & Forster, 2002; Pan et al., 2016). In particular, ozone transport within the UTLS is important because the impacts of ozone differ markedly depending on its vertical location in the atmosphere. In the stratosphere, ozone serves as a vital shield against harmful ultraviolet radiation, playing a key role in sustaining life on Earth (Crutzen, 1970; McKenzie et al., 2011; Molina & Rowland, 1974; Solomon, 1999). In contrast, in the troposphere, it acts as a major environmental pollutant that impacts human health and vegetation (Fleming et al., 2018; Monks et al., 2015). Understanding the UTLS dynamics is essential, as the transport and mixing processes in this region drive substantial ozone variability, with substantial implications for atmospheric composition and radiative forcing.

Stratosphere–troposphere exchange (STE) is a bidirectional transport process that regulates ozone distribution, water vapor balance, and radiatively active species in the UTLS (Fueglistaler et al., 2009; Holton et al., 1995; Stohl, Bonasoni, et al., 2003; Zhang et al., 2024). STE frequently occurs in the mid-latitudes when baroclinic waves are breaking (Thorncroft et al., 1993). Early studies identified tropopause folding as the primary mechanism for STE, particularly at mid-latitudes (Danielsen, 1968; Holton et al., 1995; Hoskins et al., 1985). At mid-latitudes, STE in these regions is commonly associated with Rossby wave breaking, cut-off lows, and jet stream dynamics, which facilitate the ozone transport from the stratosphere to the free troposphere (Homeyer & Bowman, 2013; Postel & Hitchman, 1999; Price & Vaughan, 1993). Downward STE transport introduces substantial amounts of ozone into the troposphere, with implications for short-term air quality and ozone-driven radiative forcing (Cooper et al., 2014; Gaudel et al., 2018; Yorks et al., 2009; Škerlak et al., 2014). These processes were noted to be most effective in springtime. However, during field campaigns with daily sonde launches over North America in 2004 and 2006 summers (Thompson et al., 2007a, 2007b, 2008), analyses of wave signatures in sonde data showed that STE influences are present after spring as well, alternating with impacts of local pollution, lightning and advected ozone in determining free tropospheric ozone structure. The classification of ozonesonde profiles with Self-Organization Maps (Stauffer et al., 2018, 2024) also pointed out that correlating vertical structure with meteorological influences is a more accurate way to interpret ozone variability than sorting by season. Ozone profiles in the tropics and subtropics are well known to exhibit signatures of STE, sometimes related to deep convection (Clain et al., 2010; Diab et al., 2004; Leclair De Bellevue et al., 2006; Portafaix et al., 2003). The convection-STE linkage has also been noted in the extratropic regions (Homeyer et al., 2014; Pan et al., 2016).

Extensive research has established a theoretical framework for STE pathways, with earlier studies identifying synoptic-scale processes as key drivers of cross-tropopause transport (Holton et al., 1995; Stohl, Wernli, et al., 2003). Climatological studies have refined this understanding by highlighting midlatitude storm tracks as hotspots for frequent tropopause folding and deep stratospheric intrusions (Sprenger et al., 2003; Škerlak et al., 2014). Observational and trajectory-based analyses have demonstrated that stratospheric ozone influx is highly variable and episodic, often modulated by regional meteorological conditions (Gettelman et al., 2011; Tarasick et al., 2019). High-frequency in situ measurements have proven essential for capturing these transient ozone transport events, reinforcing the strong influence of synoptic-scale variability on STE dynamics.

Chemical reanalysis data sets, such as the Modern-Era Retrospective Analysis for Research and Applications, Version 2 (MERRA-2; Gelaro et al., 2017) from the National Aeronautics and Space Administration (NASA) and European Centre for Medium-Range Weather Forecasts (ECMWF) Atmospheric Composition Reanalysis 4 (EAC4; Inness et al., 2019) provide long-term, globally consistent ozone distributions by assimilating satellite and in situ observations into chemical transport models. These products are widely used to investigate STE, ozone transport, and long-term atmospheric trends (Akritidis et al., 2022; Shangguan et al., 2019). They are particularly useful for complementing ozone observation networks, which have limited spatiotemporal coverage (Tarasick et al., 2021).

However, chemical reanalyses have inherent limitations, including systematic biases arising from the coarse resolution of underlying models and incomplete observational constraints, particularly under dynamically complex conditions such as STE events (Wargan et al., 2017). MERRA-2 and EAC4 have been extensively evaluated against both in situ and satellite observations (Boynard et al., 2009; Hulswar et al., 2020; Miyazaki & Bowman, 2017; Ryu & Min, 2021). These evaluations have focused on their ability to represent spatiotemporal ozone variability (Bak et al., 2022; Huijnen et al., 2020; Park et al., 2020) and dynamic processes, such as tropopause folding (Akritidis et al., 2021, 2022; Liu et al., 2020). By incorporating chemical transport models,

these data sets generally offer improved representations of ozone distribution and variability. Nevertheless, uncertainties remain in the representation of dynamic processes and short-term ozone variability, emphasizing the need for ongoing observational constraints and model refinements to improve the reliability of chemical reanalysis products.

High-resolution observations are crucial for advancing our understanding of ozone variability and STE processes. While satellites provide global coverage, their limited temporal and vertical resolutions are often insufficient for capturing the rapid and localized variations associated with STE events (Barré et al., 2012; Xu et al., 2024). In contrast, ozonesonde observations offer high vertical resolution (~100–150 m) from the surface to the lower stratosphere, making them essential instruments for investigating short-term ozone fluctuations and validating satellite and reanalysis data (Park et al., 2020; Tarasick et al., 2021).

This study aims to understand STE-driven ozone transport processes using high-resolution ozonesonde measurements obtained during the Pre-Asian Summer Monsoon Chemical and CLimate Impact Project (Pre-ACCLIP) campaign in August 2021, which is directly connected to the broader objectives of the ACCLIP (Pan et al., 2022, 2025). First, the synoptic and vertical characteristics of an ozone intrusion event are examined using the ozonesonde profiles in the UTLS. Then, the ability of two chemical reanalysis data sets to represent the vertical ozone structure and transport associated with this intrusion event is evaluated through comparison with daily in situ observations. Although long-term ozonesonde records are available at other East Asian sites with seasonal coverage, the daily high-resolution observations conducted during the Pre-ACCLIP campaign provide a unique opportunity to capture the synoptic evolution and vertical structure of the strong STE event in the summer monsoon season. Section 2 describes the data sets; Section 3 presents the observed ozone distribution and synoptic characteristics; Section 4 evaluates MERRA-2 and EAC4; Section 5 summarizes conclusion and discussion.

2. Data

2.1. Ozonesonde Observations

Ozonesondes are balloon-borne instruments that measure vertical ozone distributions with fine vertical resolution (Komhyr, 1969). Ozonesondes have a precision of 3%–5% and overall accuracy of about 5%–10% (Smit & Thompson, 2021; Tarasick et al., 2021). These in situ observations extend from the surface to the lower stratosphere and are essential for characterizing ozone variability and assessing long-term trends (Smit et al., 2007; Tarasick et al., 2021). Each ozonesonde is equipped with an electrochemical concentration cell (ECC), in which atmospheric ozone reacts with chemical solutions to generate microcurrents proportional to the ozone number concentration (Komhyr, 1969). ECC ozonesondes have been used as the global standard instrument for ozone profiling, with calibration guidelines and performance standards established by the World Meteorological Organization (WMO) Global Atmosphere Watch (GAW) program (Smit & ASOPOS, 2014; Smit et al., 2007). Progressive improvements in ozonesonde preparation and calibration have enhanced measurement accuracy and reliability (Tarasick et al., 2021; Thompson et al., 2019). Ozonesonde measurements have been performed following the Southern Hemisphere Additional Ozonesondes (SHADOZ; Thompson, Witte, et al., 2007; Thompson et al., 2017, 2019; Witte et al., 2017) preparation procedure to ensure data consistency and accuracy (Smit & ASOPOS, 2014; Smit & Thompson, 2021). Ozonesondes are launched alongside radiosondes to simultaneously measure pressure, temperature, and relative humidity, thus providing comprehensive atmospheric conditions (Stauffer et al., 2022).

In this study, ozonesonde observations were conducted at two sites in South Korea, Anmyeon (36.54°N, 126.33°E, 8 m) and Taehwa (37.31°N, 127.31°E, 30 m), as shown in Figure 1a. The Anmyeon site, located on the west coast of the Korean Peninsula, provides daily ozone profiles from 5 to 31 August 2021 during the Asia Summer Monsoon season. Ozonesondes were launched daily at 15:00 local standard time (06:00 UTC), except on 23 August when heavy rain prevented data collection. The Taehwa site served as a supplemental observation site when Anmyeon data were unavailable. A total of 26 ozone profiles were obtained, with 24 from Anmyeon and 2 from Taehwa (Figure 1b).

Most ozonesonde profiles reached approximately 33 km (~8.1 hPa), except on 8 August when the radiosonde signal was lost at around 3 km. The highest balloon burst altitude was 35.2 km on 21 August. All ozonesonde profiles were interpolated to a 100-m vertical resolution to support fine-scale analysis of ozone variability and

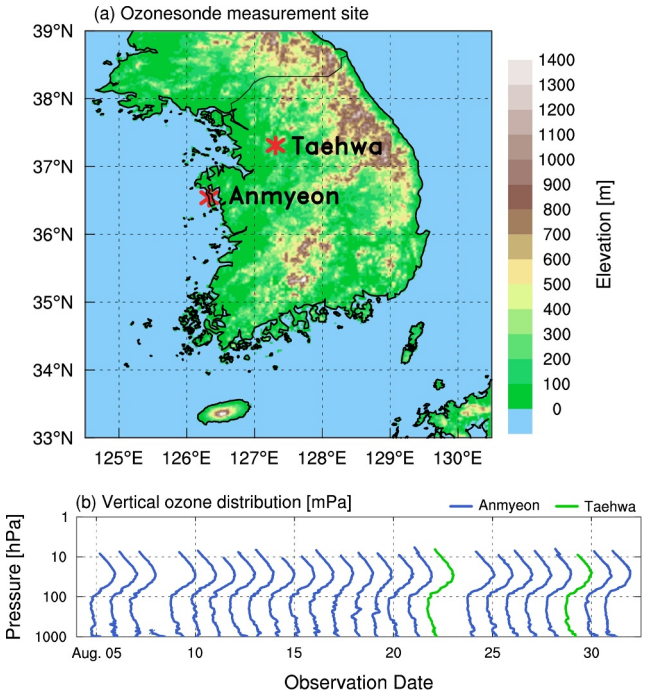

Figure 1. (a) Locations of Anmyeon (lat: 36.54°N, lon: 126.33°E, 8 m) and Taehwa (lat: 37.31°N, lon: 127.31°E, 30 m) ozonesonde measurement sites in South Korea. Shading denotes elevation (unit: m). (b) Profiles of ozone partial pressure (unit: mPa) from ozonesonde measurements at Anmyeon (blue) and Taehwa stations (green) in South Korea during pre-ACCLIP period (5–31 August 2021).

structure. Total column ozone (TCO) is also computed by vertically integrating the ozone profiles. Above the balloon burst level, the MLS-based climatology (McPeters & Labow, 2012) was appended from the burst level to the top of atmosphere, contributing 39.6 DU (Dobson Unit) on average during the campaign. One Dobson unit (DU) corresponds to a 0.01 mm thick layer of pure ozone compressed at standard temperature and pressure.

2.2. MERRA-2

MERRA-2 is NASA Global Modeling and Assimilation Office (GMAO)'s global meteorology-composition reanalysis produced with the Goddard Earth Observing System Version 5 (GEOS-5; Molod et al., 2015) at 0.5° × 0.625° horizontal resolution on 72 hybrid sigma model levels from the surface to 0.01 hPa (M2I3NVASM; Gelaro et al., 2017). MERRA-2 assimilates Solar Backscatter Ultraviolet Radiometer (SBUV and SBUV/2, Bhartia et al., 2013) partial column ozone for 1980 to September 2004. From October 2004 onward, Ozone Monitoring Instrument (OMI) total column ozone and vertical ozone profiles from the Microwave Limb Sounder (MLS) are assimilated, which substantially improved UTLS structure representation relative to the pre-Aura period (see Gelaro et al., 2017; Wargan et al., 2017). In GEOS-5, stratospheric ozone is advanced using climatological monthly two-dimensional production and loss rates based on Upper Atmosphere Research Satellite observations (Stajner et al., 2008). In contrast, tropospheric ozone has no explicit chemistry parameterization, therefore ozone behaves largely as a transported tracer with dry deposition as the primary sink (Wargan et al., 2015, 2017). To compare with ozonesonde measurements, this study uses MERRA-2 ozone field on the native model-level rather than interpolated pressure levels, which preserves the vertical resolution and structure of the original data. Ozone data are extracted from the grid points nearest to each ozonesonde launch site to ensures spatial consistency in the comparison.

2.3. EAC4

EAC4 reanalysis is a global atmospheric composition data set developed and maintained by the ECMWF using the Integrated Forecasting System (IFS, CY42R1). It provides three-dimensional fields of reactive gases, aerosols, and greenhouse gases in 3-hr intervals on a 0.75° × 0.75° horizontal grid with 60 hybrid model levels up to 0.1 hPa (Inness et al., 2019). EAC4 covers the period from 2003 to present and is continuously updated. Reactive-gas chemistry is treated online: Carbon Bond 2005 chemistry scheme (CB05) treats tropospheric chemistry within IFS (Flemming et al., 2015), while stratospheric ozone is represented by the Cariolle scheme (Cariolle and Teyssèdre, 2007). Chemical tendencies from the two schemes are merged across the diagnosed tropopause to ensure consistent coupling between chemistry and meteorology (Flemming et al., 2017). EAC4 is successor to the previous Monitoring Atmospheric Composition and Climate (MACC) reanalysis (Inness et al., 2013), and provides improvements in spatial and temporal resolution, data assimilation techniques, and model chemistry (Wagner et al., 2021). Ozone fields in EAC4 are constrained through the assimilation of satellite retrievals from multiple instruments, including TCO from OMI and Global Ozone Monitoring Experiment-2, vertical profiles from MLS, partial columns from SBUV/2, and profile and column data from Infrared Atmospheric Sounding Interferometer (IASI; Boynard et al., 2009; Inness et al., 2019). Surface and fire emission are taken from MACCity anthropogenic (Granier et al., 2011) and GFAS v1.2 daily biomass burning emissions (Kaiser et al., 2012). Biogenic emissions from MEGAN2.1 (Guenther et al., 2006), and selected natural sources are employed in IFS-CB05 (Flemming et al., 2017). For this study, ozone field were extracted from the native model-level at 06 UTC for the grid points nearest to each ozonesonde launch location.

2.4. ERA5 and Satellites

Additionally, the ECMWF Reanalysis v5 (ERA5), developed by the ECMWF, is used to analyze synoptic-scale meteorological conditions relevant to STE events (Hersbach et al., 2020). Geopotential height (GPH), wind, and

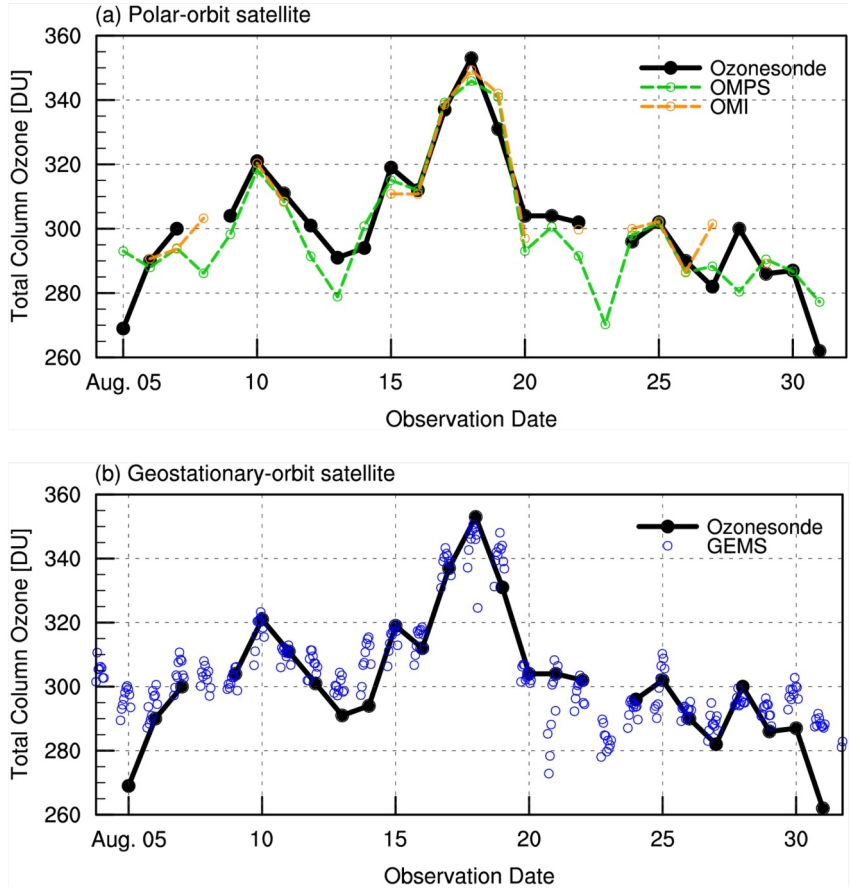

Figure 2. Time series of total column ozone (unit: DU) from ozonesonde measurements (black solid line), (a) polar-orbit satellites (dashed lines; OMPS: green, OMI: orange), and (b) geostationary-orbit satellite (GEMS: blue).

potential vorticity (PV) fields are analyzed to characterize UTLS dynamical structures relevant to ozone transport. For TCO time series, three satellite instruments were used to compare the TCO with ozonesonde measurements: Ozone Mapping and Profiler Suite (OMPS, Flynn et al., 2014; Jaross et al., 2014), OMI (Kroon et al., 2011; Levelt et al., 2006; McPeters et al., 2008), and Geostationary Environment Monitoring Spectrometer (GEMS, Bak et al., 2013; Kim et al., 2020). For the polar-orbiting instruments (OMPS/OMI), daily gridded TCO data from the NOAA Global Monitoring Division (https://gml.noaa.gov/grad/neubrew/SatO3DataTimeSeries.jsp, last access: 29 September 2025) were used. The point values were computed from the gridded data using a bi-linear interpolation. For GEMS, which provides hourly daytime TCO with high horizontal resolution (Δx: 7–8 km; Kim et al., 2020), the nearest value at 06 UTC were used for day-to-day comparison.

3. Observed STE Structure

Figure 2 presents the day-to-day TCO variability from ozonesondes and the three satellites products (OMPS, OMI, and GEMS) throughout August 2021. The strong consistency between the data sets confirms the reliability of both the balloon-borne and satellite-based ozone measurements. The TCO ranged between 262 and 353 DU, with an average of 301 DU, which closely aligns with the long-term August mean of ∼295 DU recorded in South Korea (Pohang ozonesonde station, Shin et al., 2020). A significant TCO enhancement of approximately 40 DU was observed between 16 and 18 August peaking at 353 DU on 18 August. This sharp increase was consistently captured by all satellites. Such temporal variability in TCO is typically driven by synoptic-scale weather patterns that are related to transport and mixing processes (Akritidis et al., 2018; Greenslade et al., 2017; Trickl et al., 2010).

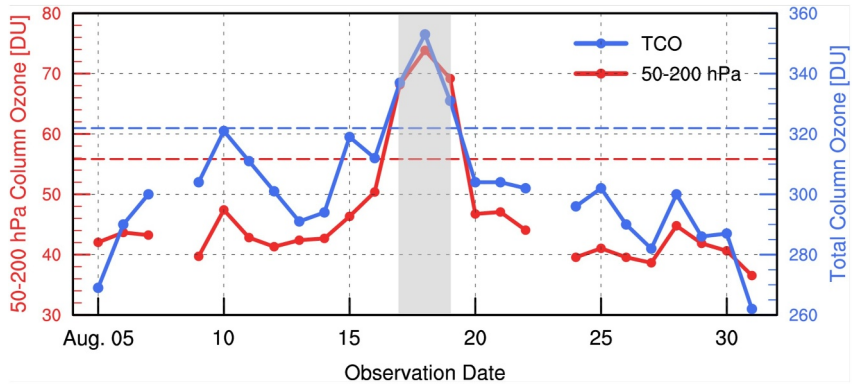

Figure 3. Time series of ozonesonde total (blue solid line) and 50–200 hPa (red solid line) column ozone (unit: DU). Horizontal dashed lines present the standard deviation of total (blue, 321.9 DU) and 50–200 hPa (red, 55.8 DU) column ozone, respectively. Gray shading indicates the stratosphere-troposphere exchange periods.

To further investigate the source of this enhancement, Figure 3 compares the TCO and the 50–200 hPa layer (hereafter referred to as the UTLS) column ozone. The UTLS ozone closely mirrored the TCO temporal pattern, with a pronounced peak on 18 August which coincides with the TCO maximum. Notably, this UTLS layer exhibits the greatest variability throughout the observation period, indicating that ozone changes in this region significantly influence TCO variabilities. The UTLS ozone increased by over 23 DU during this period, accounting for approximately 60% of the TCO enhancement. This result aligns with previous findings highlighting the key role of UTLS processes in TCO variability (Gettelman et al., 2011; Hoor et al., 2010). This contribution on daily variability implies that synoptic-scale atmospheric processes are involved in the UTLS transport and mixing. The observed enhancement is related to STE, through which ozone-rich stratospheric air intrudes into the troposphere (Holton et al., 1995; Stohl, Bonasoni, et al., 2003; Škerlak et al., 2014). Although STE events are more frequent in winter and spring due to stronger baroclinicity (Akritidis et al., 2021; Sprenger et al., 2003), this summer event exhibits a comparably deep and strong ozone intrusion (Figure 4) This event is also scientifically valuable because the fine temporal resolution of the ozonesonde measurements helps to clearly capture the structure and timing of the STE process.

Figure 4 presents the time-height cross section of ozone mixing ratio (unit: ppbv) from ozonesonde measurements during the observation period. The thick black contour highlights the 100 ppbv level, which serves as a visual threshold to distinguish ozone-rich air masses. The lapse-rate defined tropopause is marked with green dots (World Meteorological Organization, 1957) to indicate the boundary between the stratosphere and troposphere. Enhanced ozone concentrations were distinctly observed in the mid-to-upper troposphere between 17 and 19 August temporally coinciding with the TCO maximum in Figure 2. During this period, ozone mixing ratios exceeded 100 ppbv and locally reached up to 560 ppbv below the tropopause. These values are substantially higher than the typical summertime range of 80–100 ppbv in mid-to-upper troposphere over the mid-latitude regions, including South Korea (Gaudel et al., 2018; Zbinden et al., 2013). This substantial enhancement represents a significant deviation from the seasonal ozone variability, indicating that this enhancement was most likely driven by a stratospheric intrusion rather than regional photochemical processes. This result is further supported by the simultaneous time-height cross section of relative humidity (RH; see Figure S3 in Supporting Information S1), which reveals the descent of extremely dry air from the upper troposphere to the mid-troposphere during the period. This concurrent feature of high ozone and low RH strongly indicates that the air has a stratospheric origin (e.g., Müller et al., 2024).

To examine the impact of the stratospheric air intrusion on the vertical ozone structure, the ozonesonde profiles are categorized into the STE and background cases, as shown in Figure 3. Days with both TCO and UTLS column ozone values exceeding their respective one standard deviation (+1 σ) thresholds were defined as STE cases, corresponding to 17, 18, and 19 August. Figure 5 shows the vertical ozone distributions for those cases. A distinct difference between the STE and background cases appears in the UTLS (50–200 hPa), where ozone partial pressures are significantly higher during the STE event (Figure 5a). A prominent secondary ozone peak (SOP; Hwang et al., 2007; Hoor et al., 2010; Park et al., 2012) was observed within the UTLS, with a maximum mean ozone partial pressure of ~6 mPa, and it coincided with the region of greatest standard deviation (Figure 5c; at

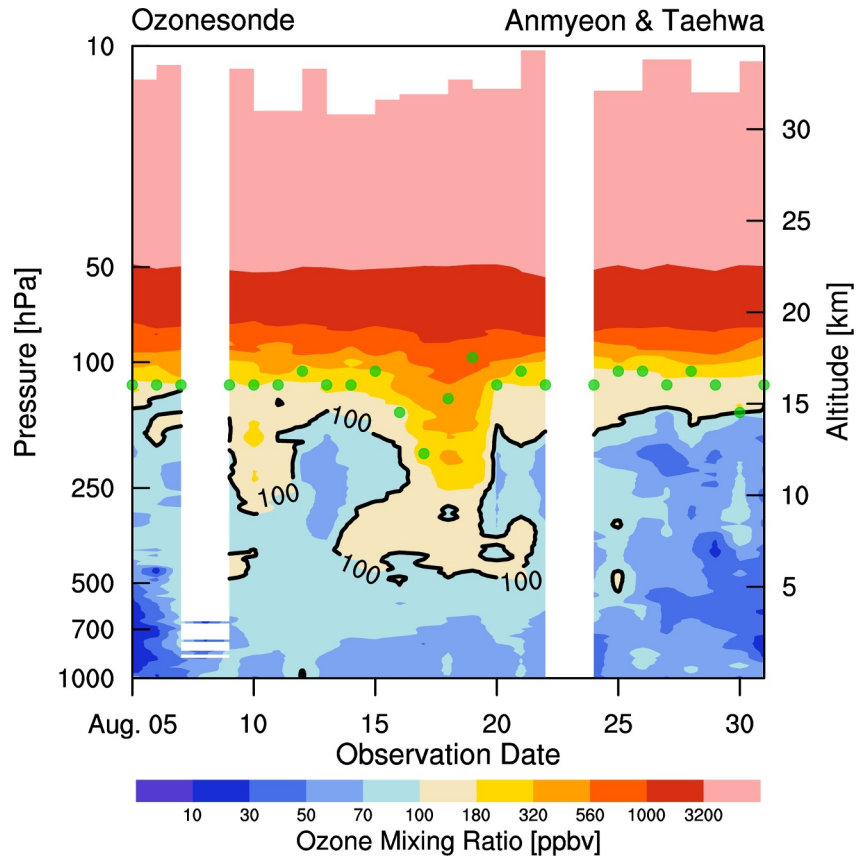

Figure 4. Time-height cross section of ozone mixing ratio (shading, unit: ppbv) from ozonesonde measurements. The black contour indicates the 100 ppbv level. The green dots represent the lapse-rate tropopause defined by World Meteorological Organization (1957).

~200 hPa). The SOP represents stratospheric ozone intruding into the upper troposphere isentropic surfaces during tropopause folding (Holton et al., 1995). This intrusion not only reshapes the vertical ozone profile but also contributes significantly to the observed increase in TCO. Rossby wave breaking contributes to the downward mixing of ozone-rich air masses from the lower stratosphere, thereby facilitating the formation of SOPs

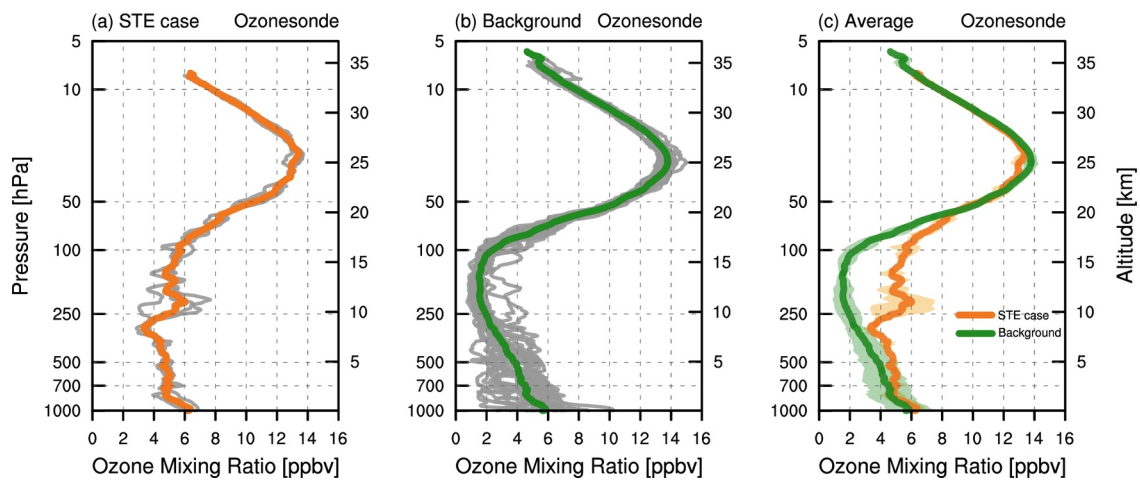

Figure 5. Vertical profiles of ozone partial pressure (unit: mPa) from ozonesonde measurements for (a) STE case, (b) background, and (c) their averages. Thick orange and green lines indicate the mean profiles for each case. Thin gray lines show the individual profiles. Orange and green shadings indicate one standard deviation (±1 σ).

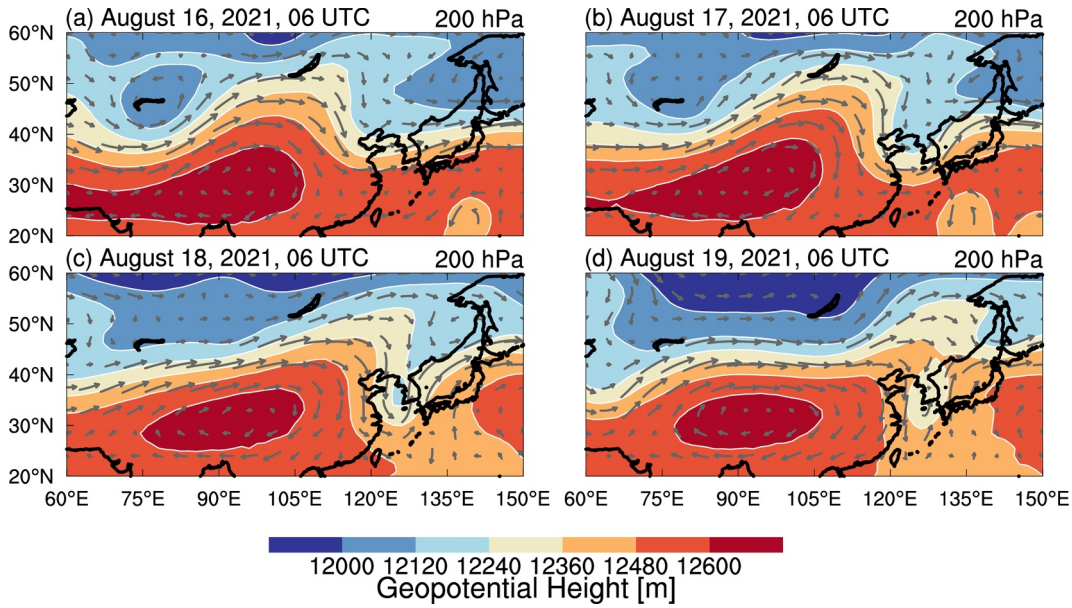

Figure 6. Spatial distributions of 200-hPa geopotential height (shading, unit: m) and wind (gray vector, unit: m s^{-1}) fields over Asia from ERA5 reanalysis at 06 UTC (15 KST) (a) 16, (b) 17, (c) 18, and (d) 19 August 2021.

(Lemoine, 2004; Reid & Vaughan, 1991). This dynamically driven deformation intrusion of ozone-rich lower stratospheric air into the upper troposphere leads to the formation of a SOP in the UTLS region (Park et al., 2012). Since this additional ozone is incorporated into the TCO, the occurrence of SOPs is closely linked to observed TCO enhancements. Therefore, identifying SOP signatures in vertical ozone profiles provides insight into the strength of Rossby wave breaking and the associated STE activity.

The synoptic-scale evolution of the STE event is analyzed using the GPH (Figure 6) and PV (Figure 7) at 200 hPa from 16 to 19 August. Figure 6 shows the progressive deepening of an upper-level trough over northeastern China and Korea with an expanding anticyclone, which is known as the Asia summer monsoon anticyclone (Pan et al., 2016, 2024). On 18 August a notable cut-off low developed over the Korean Peninsula, coinciding with a

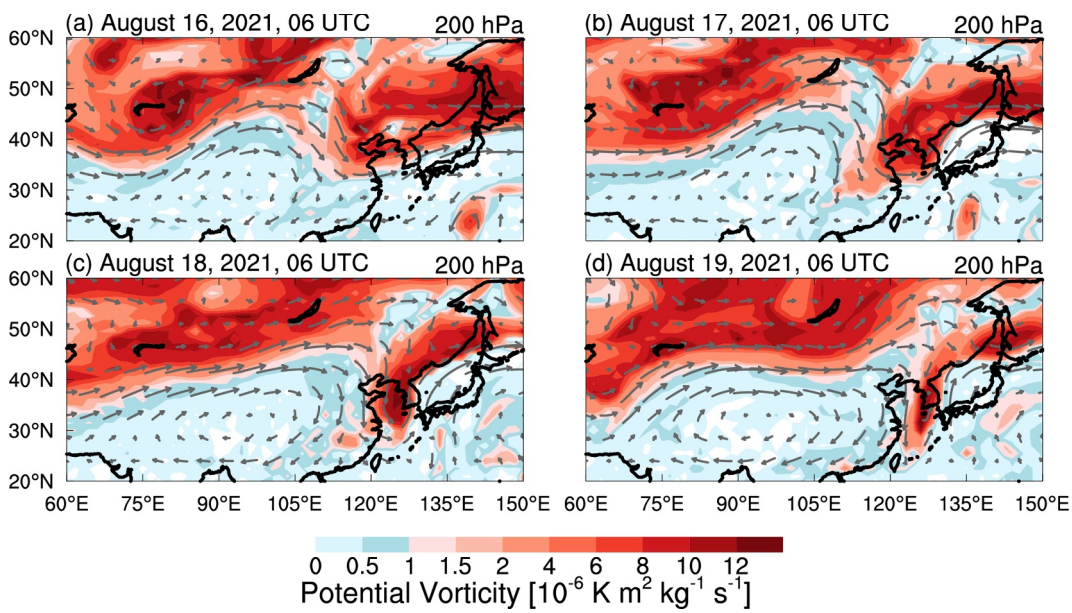

Figure 7. Same as in Figure 6, but for potential vorticity at 200-hPa (unit: 10^{-6} K m^2 kg^{-1} s^{-1}).

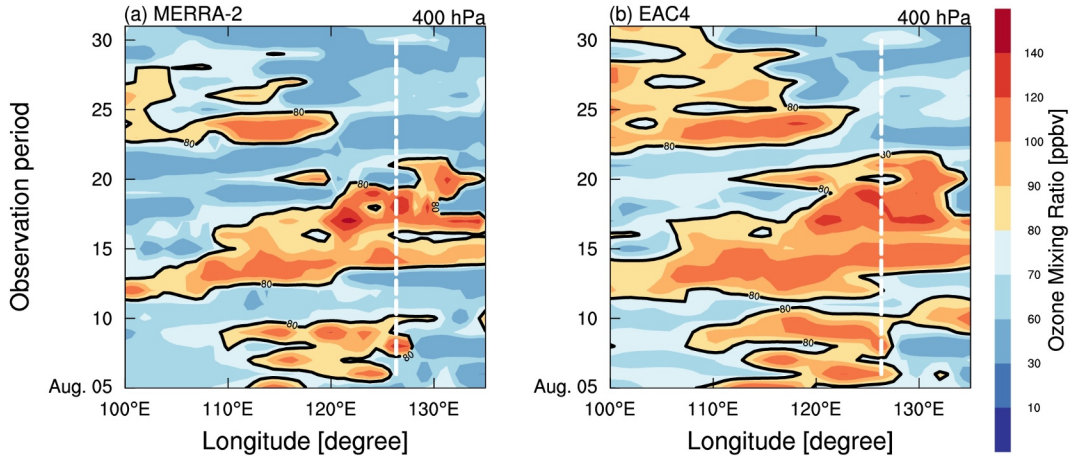

Figure 8. Hovmöller diagrams of the ozone mixing ratio (shading, unit: ppbv) from (a) MERRA-2 and (b) EAC4 at 400 hPa. Black solid line indicates 80 ppbv. White dashed line indicates the longitude of Anmyeon station (126.33°E).

local high in PV (Figures 6c, 6d, 7c and 7d). Since PV is a conserved quantity under adiabatic conditions (Danielsen, 1968), its spatial distribution is frequently used to trace the air-mass origin and identify dynamical tropopause (Holton et al., 1995). Notably, stratospheric air masses are characterized by significantly higher PV values (typically >2 PVU) than those in the troposphere. Therefore, the presence of enhanced PV at 200 hPa supports the inference of stratospheric intrusion into the upper troposphere via tropopause folding (Sprenger et al., 2003; Škerlak et al., 2014). The large-scale GPH and PV patterns closely resemble the structure of anti-cyclonic Rossby wave-breaking (AWB), as described by Thorncroft et al. (1993). Such wave breaking enhances the downward transport of stratospheric air and facilitates STE processes. While both cyclonic and anticyclonic wave breaking can contribute to STE, the observed wave pattern during this period displays a clear anticyclonic signature along the northern edge of the Asian summer monsoon anticyclone. Hence, this observed STE event is interpreted as dynamically linked to AWB. The relationship between enhanced PV and stratospheric air intrusion is well-documented in Thouret et al. (2006), which reported a strong spatial correlation between ozone volume mixing ratios and potential vorticity in the UTLS region based on the MOZAIC (Measurement of Ozone and Water Vapor by Airbus In Service Aircraft) data. Our result is consistent with the previous findings and reinforces the link between STE events and enhanced PV signatures.

Figure 4 reveals that elevated ozone levels (>100 ppbv) were also observed in the mid-to-upper troposphere even prior to the main STE event. To further investigate this enhanced ozone structure, the temporal evolution of the ozone distribution is investigated using two chemical reanalyses. Figure 8 presents Hovmöller diagrams of the ozone mixing ratio at 400 hPa for MERRA-2 and EAC4. Both reanalyses show eastward-propagating band of elevated ozone (>80 ppbv) extending from Eastern China (~100°E) toward the Korean Peninsula, particularly during 10–20 August. This band coincides with the enhanced ozone detected at Anmyeon station (white line in Figure 8), suggesting large-scale horizontal transport of ozone-rich air likely occurs in the mid-troposphere by mid-latitude westerlies (Lelieveld & Dentener, 2000; Trickl et al., 2003). A similar spatiotemporal pattern is also found in relative humidity fields at 400 hPa, which coincide well with high ozone values (see Figure S8 in Supporting Information S1). These findings suggest that the enhanced TCO observed during the campaign period was influenced by both vertical intrusion through tropopause folding and horizontal advection of air with stratospheric origin. In particular, the ozone enhancement observed around 16–18 August likely reflects the combined effect of both mechanisms. This highlights the importance of simultaneously considering both vertical and horizontal transport pathways when interpreting ozone variability in the upper and middle troposphere, especially during dynamically active synoptic events.

4. Comparison to Chemical Reanalyses

To evaluate the ability of chemical reanalysis products to capture synoptic-scale ozone variability during the campaign period, Figure 9 presents the time-height distribution of the ozone mixing ratios from MERRA-2 and EAC4. The hatched regions indicate the 100–320 ppbv ozone range from the ozonesonde measurements (see

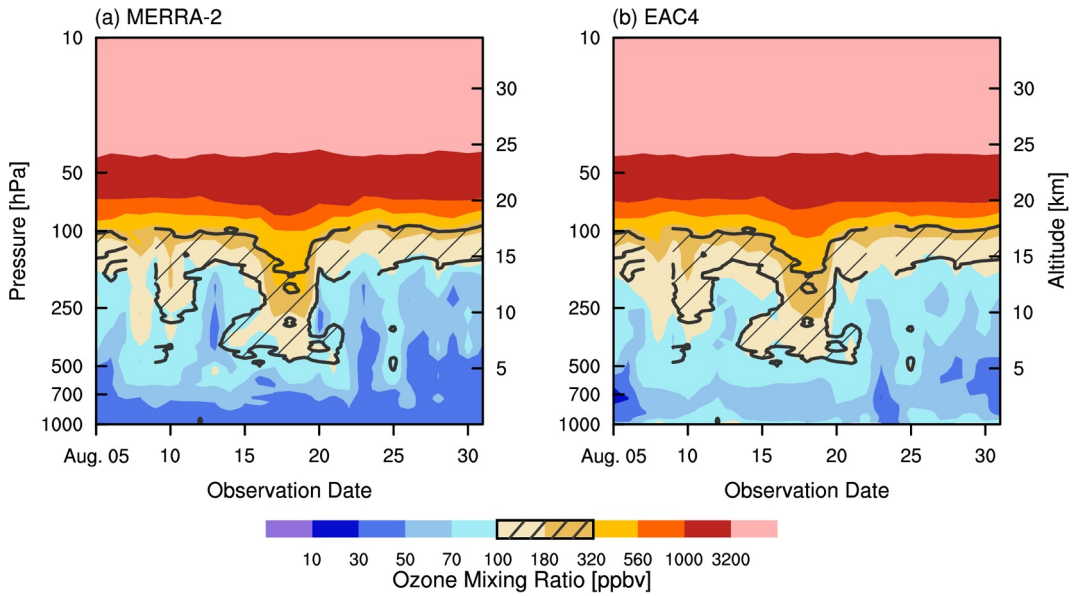

Figure 9. Same as in Figure 4, but for (a) MERRA-2 and (b) EAC4 chemical reanalyses. The hatching indicates 100–320 ppbv area from ozonesonde measurements (see Figure 4).

Figure 4), corresponding to the approximate region of the ozone intrusion. MERRA-2 and EAC4 successfully reproduce the key structural features of the STE event, including the downward intrusion of high-ozone air masses into the upper troposphere. In the stratosphere, ozone distributions both reanalyses closely follow the vertical structure and magnitude observed in the ozonesonde measurements (see Figure 10 for quantitative comparison). However, notable differences emerge in the troposphere. MERRA-2 generally underestimates ozone mixing ratios compared to both EAC4 and ozonesonde profiles, particularly in the lower and mid troposphere.

To further quantify these differences in ozone distribution, the vertical profiles of the ozone partial pressure are examined for the STE and background cases. Both reanalyses generally reproduce the vertical ozone structure seen in the ozonesonde, particularly in the stratosphere, where the variability is low (Liu et al., 2020; Shangguan et al., 2019). However, significant differences emerge in the UTLS region. During the STE case (Figure 10a), strong ozone variability appears in the UTLS, which coincided with the SOP structure. MERRA-2 captures this SOP structure more distinctly than EAC4, showing well-defined ozone peak centered around 200 hPa that closely aligns with ozonesonde profiles. In contrast, EAC4 exhibits a relatively smooth and distribution with minimal vertical structure from 500 hPa up to 100 hPa, with a less distinct representation of the SOP feature. In the lower troposphere, MERRA-2 underestimates ozone concentrations, while EAC4 generally agrees better with the ozonesonde measurements.

The differences between MERRA-2 and EAC4 in representing ozone distribution are likely influenced by data assimilation systems as well as how chemical and emissions processes are represented within each model framework. A fundamental distinction between MERRA-2 and EAC4 is that MERRA-2 does not include ozone chemistry in the troposphere, instead relying on satellite data assimilation and transport processes with dry deposition (Wargan et al., 2015, 2017). As a result, the discrepancies in the reanalysis of the tropospheric ozone are more likely to originate from differences in chemical processes. Although both reanalyses assimilate MLS data, which provides a large volume of ozone information above ~215 hPa (McPeters & Labow, 2012; Ziemke et al., 2011), ozone in the middle and lower tropospheric remains weakly constrained due to the limited availability of direct observation. EAC4 treat tropospheric ozone explicitly using the CB05 chemistry scheme along with high spatial and temporal resolution anthropogenic and biomass burning emissions (Inness et al., 2019; Wagner et al., 2021). These features likely contribute to its better agreement with ozonesonde measurements in the lower troposphere. However, EAC4 consistently overestimates near-surface ozone concentrations, which may stem from biases in emissions or chemical reactivity. In contrast, MERRA-2 tends to underestimate lower tropospheric ozone but better resolves upper-level features such as the SOP.

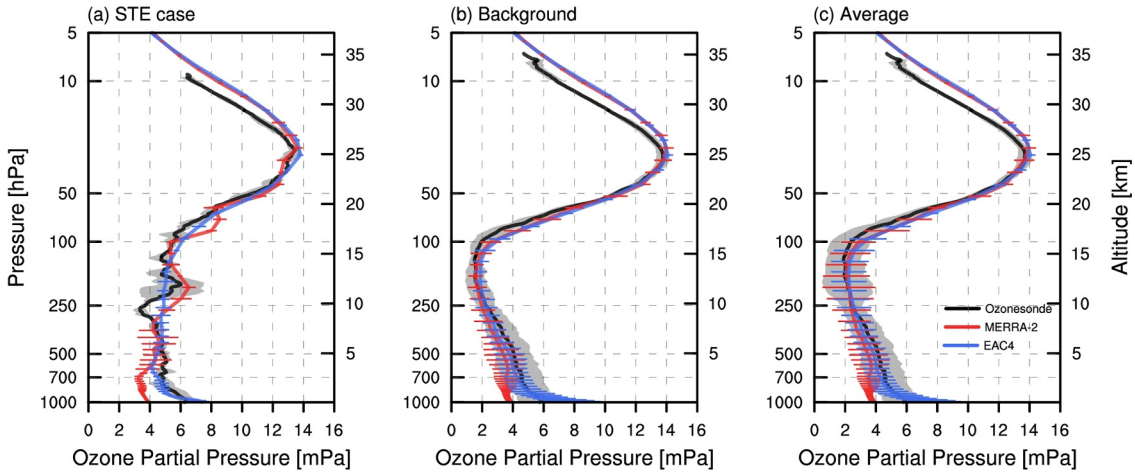

Figure 10. Mean vertical profiles of ozone partial pressure (unit: mPa) from ozonesonde (black), MERRA-2 (red), and EAC4 (blue) for (a) STE case, (b) background and (c) their averages. Gray shading indicates one standard deviation (±1 σ) of ozonesonde measurements. The red and blue horizontal lines indicate ±1 σ of MERRA-2 and EAC4, respectively.

To assess the performance of the reanalysis data in reproducing observed TCO, integrated TCO values derived from MERRA-2 and EAC4 vertical profiles are compared with ozonesonde measurements (e.g., Figure 11). The reanalysis TCOs are computed by vertically integrating ozone mixing ratio from the surface to 1 hPa. Both reanalyses exhibit strong agreement with the observed TCO, with squared correlation coefficients (r^2) of 0.88 for MERRA-2 and 0.90 for EAC4. These high correlation value indicate that both reanalyses effectively capture the overall temporal evolution of column ozone. In terms of average TCO, MERRA-2 shows a mean value of 301.6 DU, closely aligned with the ozonesonde mean of 301.9 DU. In contrast, EAC4 yields a higher mean value of 311.7 DU, suggesting a positive bias relative to the observed TCO. The scatterplot also shows that MERRA-2 has a steeper regression slope (0.90) than EAC4 (0.81), suggesting different sensitivities to daily ozone variations.

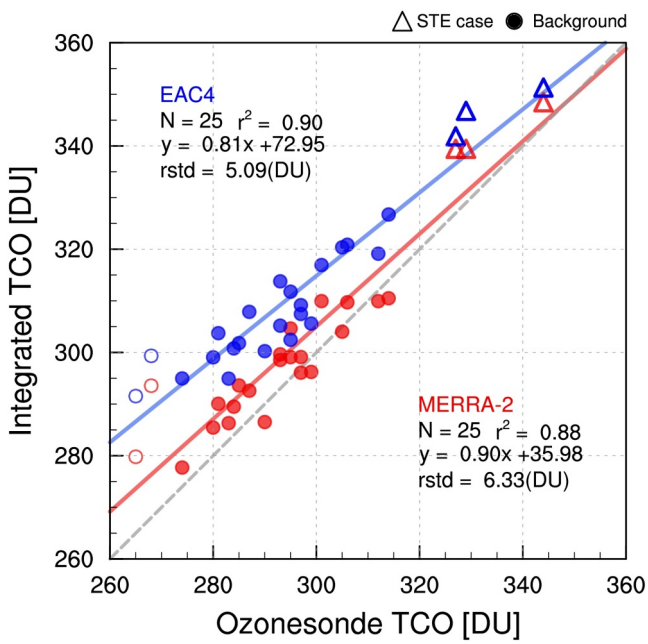

Figure 11. Scatter plot with regression lines of total column ozone from MERRA-2 (red) and EAC4 (blue) against ozonesonde measurements. Triangles and circles present the STE case and background, respectively.

The regression slope difference between the two reanalyses also reflects how each reanalysis responds to synoptic-scale ozone variability. MERRA-2 has a higher slope (0.90) compared to EAC4 (0.81), suggesting higher responsiveness to synoptic-scale ozone fluctuations. The residual standard deviation (rstd) further supports this interpretation. MERRA-2 shows a larger rstd (6.33 DU) than EAC4 (5.09 DU), indicating that while it tracks short-term variability more closely, it also exhibits greater scatter. EAC4, in contrast, demonstrates a smoother regression fit with reduced sensitivity to high-frequency changes. To test the robustness of these patterns, two anomalously low TCO values observed on 5 and 31 August —when ozonesonde measurements diverged markedly from satellite-based TCO products (e.g., OMPS and GEMS; see Figure 2)—were excluded from the analysis. As shown in Figure S13 in Supporting Information S1, this pattern could be improved (Figure S13 in Supporting Information S1; MERRA-2: 1.01, EAC4: 0.88) without two days with unusually low TCO values (5 and 31 August; marked with open circles). This difference persists even after excluding the two lowest TCO values, though the gap narrows to approximately 1 DU. Both reanalyses demonstrate similarly strong accuracy in reproducing temporal evolution of TCO, MERRA-2 shows a stronger response to daily variability, whereas EAC4 provides a smoother but systematically biased representation.

To quantitatively assess the vertical contributions to the observed TCO biases, column ozone is integrated over three atmospheric layers: the stratosphere (1–150 hPa), the troposphere (150–1,000 hPa), and the UTLS (50–200 hPa). Figure 12 presents the time series of layer-specific column ozone

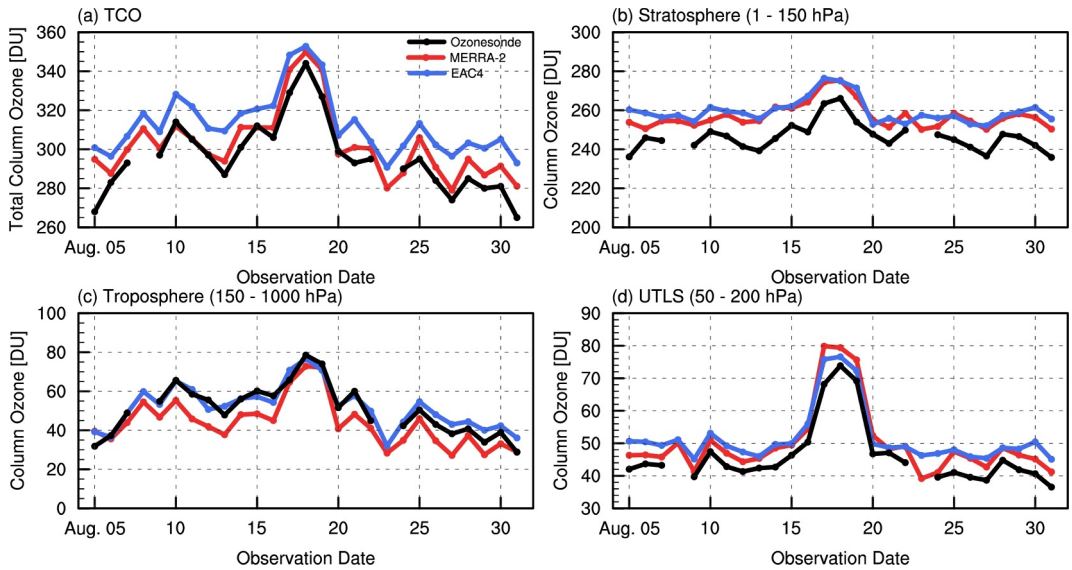

Figure 12. Time series of (a) total column ozone and column ozone in the (b) stratosphere, (c) stratosphere, and (d) upper troposphere-lower stratosphere from ozonesonde measurements (black), MERRA-2 (red), and EAC4 (blue).

from ozonesonde measurements, MERRA-2, and EAC4. As shown in Figure 12a, EAC4 persistently overestimates TCO throughout the entire observation period. A similar amount of overestimation (~20 DU) appeared in the stratospheric column for EAC4 (Figure 12b), suggesting that the TCO bias in EAC4 originates predominantly from this layer. MERRA-2 also shows the same overestimation, which is largely offset by the tropospheric underestimation. It is worth to note that ozonesonde uses MLS-based climatology above ~7 hPa to compute the stratospheric column, however it doesn't affect the bias pattern. In contrast, EAC4 exhibits relatively good agreement with ozonesonde values in the troposphere (Figure 12c), minimally contributing to the TCO bias. For MERRA-2, a similar overestimation is present in the stratosphere, but it also underestimates in the troposphere. Although a negative bias is present in the troposphere, its magnitude is insufficient to fully compensate for the stratospheric overestimation, resulting in a residual positive bias in the TCO. MERRA-2 tends to overestimate ozone concentrations compared to ozonesonde data in the UTLS layer (Figure 12d), despite an overall tropospheric underestimation. The remaining TCO bias from MERRA-2 appears to result from combined overestimation in the UTLS and the lower stratosphere, both of which exhibit systematic positive biases relative to ozonesonde observations.

The detailed vertical structure (Figure 10) reveals that ozone in both reanalyses is distributed more broadly in the stratosphere compared to ozonesonde measurements. As a result, overestimations mainly occur near the lowermost stratosphere (~100 hPa) and mid-stratosphere (~10 hPa), which correspond to the lower and upper boundaries of the ozone layer. These discrepancies are consistent with previous studies that reanalyses tend to introduce stratospheric ozone biases due to differences in data assimilation techniques and model representations of transport and chemistry (Randel & Wu, 2007). In particular, the use of averaging kernels in satellite data assimilation likely alters the vertical sensitivity of ozone, leading to layer-dependent positive biases in the stratosphere (Rodgers & Connor, 2003; Verhoelst et al., 2015). The UTLS region, where steep gradients and satellite assimilation uncertainties are more prevalent, shows particularly pronounced overestimation (Figure 12d). These results suggest that residual biases in TCO are primarily driven by systematic overestimation in the stratosphere.

5. Conclusions

This study examined synoptic-scale ozone variability by combining daily ozonesonde measurements with MERRA-2 and EAC4 chemical reanalyses, focusing on the summertime STE event and associated regional-scale ozone transport. A pronounced TCO enhancement was observed between 17 and 19 August with the ozonesonde measurements revealing that more than half of the increase (~60%) originated from the UTLS. Dynamical analysis identified anticyclonic Rossby wave breaking, cut-off lows, and associated tropopause folding as the key

mechanisms driving the downward transport of stratospheric ozone into the troposphere. This is supported by the coincident patterns of low relative humidity and elevated PV, which are characteristic tracers of stratospheric air. Additionally, horizontal advection in the middle troposphere also partly contributed to the ozone enhancement. These results reveal that the high ozone event in UTLS was driven by STE process with partial support of horizontal advection.

Both reanalysis data sets qualitatively reproduced the STE structure and captured the day-to-day ozone variability in the UTLS. This ozone variability in the UTLS could potentially be reproduced by the model itself in the reanalysis system because numerical weather prediction models can simulate upper tropospheric Rossby wave breaking. However, the strength of mixing by Rossby wave breaking could be different in models. For example, MERRA-2 exhibits stronger PV enhancement compared to EAC4 during the event (see Figure S12 in Supporting Information S1). Thus, the difference in UTLS ozone structure is more likely due to the simulated STE strength. EAC4 presents smoother vertical structure (Figure 10). Although satellite data assimilation and chemical parameterization could also affect the day-to-day ozone variations in the UTLS, their impacts look secondary.

Systematic biases in the reanalysis of ozone fields remain evident across different atmospheric layers and are shaped by differences in satellite data assimilation and model constraints. Both MERRA-2 and EAC4 overestimated stratospheric ozone, likely owing to vertical smoothing effects in satellite retrievals and differences in how stratospheric profiles are assimilated. These biases propagate into the TCO estimates. Reducing these discrepancies will require improved treatment of model error structures, background covariance, and the assimilation of vertically resolved observations.

In the troposphere, differences between two reanalyses appear to be influenced by their chemistry and emission treatments. MERRA-2 is yet to include tropospheric chemistry. This likely leads to the persistent underestimation of ozone in the lower and middle troposphere (Huijnen et al., 2020; Wargan et al., 2015, 2017). Conversely, EAC4 exhibits a persistent positive bias near the surface, which is potentially linked to the model treatment of precursor emissions and chemical reactivity parameterization that influence ozone formation rates (Wagner et al., 2019). These findings are consistent with prior intercomparison studies and underscore the need to assimilate both ozone and its chemical precursors to improve tropospheric ozone accuracy (Sekiya et al., 2025). Overall, these results demonstrate that the quality of ozone data in chemical reanalysis is influenced by multiple factors: the assimilation of satellite observation, the dynamical transport near the tropopause, and the tropospheric chemistry and emission inventories.

Finally, this study highlights the critical value of high-resolution daily ozone profile measurements are essential for advancing chemical reanalysis accuracy and improving model performance. in situ observations provide fine-scale ozone changes, particularly during dynamically active events such as STE and large-scale transport, which are often insufficiently resolved by models or satellite retrievals. However, the operational demands and cost of such measurements limit their widespread implementation. The sustained implementation of specialized field campaigns, such as ACCLIP, is vital for expanding access to high-quality vertical ozone information, ultimately improving the representation of atmospheric composition in global reanalyses.

Conflict of Interest

The authors declare no conflicts of interest relevant to this study.

Data Availability Statement

Ozonesonde data used in this study were obtained from the Pre-ACCLIP (2021) campaigns and are publicly available from the Earth Observing Laboratory (EOL) of the National Center for Atmospheric Research (NCAR) data archive (Kim & Koo, 2024). MERRA-2 reanalysis data used in this study are available from the NASA Goddard Earth Sciences Data and Information Services Center (GES DISC) at (GMAO, 2015). The CAMS global reanalysis data (EAC4) are provided by (Copernicus Atmosphere Monitoring Service, 2020). ERA5 reanalysis data from the European Centre for Medium-Range Weather Forecasts (ECMWF) are available at (Copernicus Climate Change Service, Climate Data Store, 2023). All data sets used in this study are publicly accessible.

Acknowledgments
This study was supported by the National Institute of Environmental Research funded by the Ministry of Climate, Energy and Environment (MCEE) of the Republic of Korea (NIER-2022-01-02-045, NIER-2024-01-01-005, NIER-2021-03-03-007) and the Specialized university program for confluence analysis of Weather and Climate Data of the Korea Meteorological Institute (KMI) funded by the Korean government (KMA). We are deeply grateful to three anonymous reviewers for their insightful and constructive comments, which greatly improved the manuscript.

References

Akritidis, D., Katragkou, E., Zanis, P., Pytharoulis, I., Melas, D., Flemming, J., et al. (2018). A deep stratosphere-to-troposphere ozone transport event over Europe simulated in CAMS global and regional forecast systems: Analysis and evaluation. *Atmospheric Chemistry and Physics*, *18*(20), 15515–15534. https://doi.org/10.5194/acp-18-15515-2018

Akritidis, D., Pozzer, A., Flemming, J., Inness, A., Nédélec, P., & Zanis, P. (2022). A process-oriented evaluation of CAMS reanalysis ozone during tropopause folds over Europe for the period 2003–2018. *Atmospheric Chemistry and Physics*, *22*(9), 6275–6289. https://doi.org/10.5194/acp-22-6275-2022

Akritidis, D., Pozzer, A., Flemming, J., Inness, A., & Zanis, P. (2021). A global climatology of tropopause folds in CAMS and MERRA-2 reanalyses. *Journal of Geophysical Research: Atmospheres*, *126*(8), e2020JD034115. https://doi.org/10.1029/2020JD034115

Bak, J., Kim, J. H., Liu, X., Chance, K., & Kim, J. (2013). Evaluation of ozone profile and tropospheric ozone retrievals from GEMS and OMI spectra. *Atmospheric Measurement Techniques*, *6*(2), 239–249. https://doi.org/10.5194/amt-6-239-2013

Bak, J., Song, E.-J., Lee, H.-J., Liu, X., Koo, J.-H., Kim, J., et al. (2022). Temporal variability of tropospheric ozone and ozone profiles in the Korean Peninsula during the East Asian summer monsoon: Insights from multiple measurements and reanalysis datasets. *Atmospheric Chemistry and Physics*, *22*(21), 14177–14187. https://doi.org/10.5194/acp-22-14177-2022

Barré, J., Peuch, V.-H., Attié, J.-L., El Amraoui, L., Lahoz, W. A., Josse, B., et al. (2012). Stratosphere-troposphere ozone exchange from high resolution MLS ozone analyses. *Atmospheric Chemistry and Physics*, *12*(14), 6129–6144. https://doi.org/10.5194/acp-12-6129-2012

Bhartia, P. K., McPeters, R. D., Flynn, L. E., Taylor, S., Kramarova, N. A., Frith, S., et al. (2013). Solar backscatter UV (SBUV) total ozone and profile algorithm. *Atmospheric Measurement Techniques*, *6*(10), 2533–2548. https://doi.org/10.5194/amt-6-2533-2013

Boynard, A., Clerbaux, C., Coheur, P.-F., Hurtmans, D., Turquety, S., George, M., et al. (2009). Measurements of total and tropospheric ozone from IASI: Comparison with correlative satellite, ground-based and ozonesonde observations. *Atmospheric Chemistry and Physics*, *9*(16), 6255–6271. https://doi.org/10.5194/acp-9-6255-2009

Cariolle, D., & Teyssedre, H. (2007). A revised linear ozone photochemistry parameterization for use in transport and general circulation models: Multi-annual simulations. *Atmospheric Chemistry and Physics*, *7*(9), 2183–2196. https://doi.org/10.5194/acp-7-2183-2007

Clain, G., Baray, J.-L., Delmas, R., Keckhut, P., & Cammas, J.-P. (2010). A lagrangian approach to analyse the tropospheric ozone climatology in the tropics: Climatology of stratosphere–troposphere exchange at Reunion Island. *Atmospheric Environment*, *44*(7), 968–975. https://doi.org/10.1016/j.atmosenv.2009.08.048

Cooper, O. R., Parrish, D. D., Ziemke, J., Balashov, N. V., Cupeiro, M., Galbally, I. E., et al. (2014). Global distribution and trends of tropospheric ozone: An observation-based review. *Elementa*, *2*, 000029. https://doi.org/10.12952/journal.elementa.000029

Copernicus Atmosphere Monitoring Service. (2020). CAMS global reanalysis (EAC4) [Dataset]. *Copernicus Atmosphere Monitoring Service (CAMS) Atmosphere Data Store*. https://doi.org/10.24381/d58bbf47

Copernicus Climate Change Service, Climate Data Store. (2023). ERA5 hourly data on single levels from 1940 to present [Dataset]. *Copernicus Climate Change Service (C3S) Climate Data Store (CDS)*. https://doi.org/10.24381/cds.adbb2d47

Crutzen, P. J. (1970). The influence of nitrogen oxides on the atmospheric ozone content. *Quarterly Journal of the Royal Meteorological Society*, *96*(408), 320–325. https://doi.org/10.1002/qj.49709640815

Danielsen, E. F. (1968). Stratospheric–tropospheric exchange based on radioactivity, ozone and potential vorticity. *Journal of the Atmospheric Sciences*, *25*(3), 502–518. https://doi.org/10.1175/1520-0469(1968)025<0502:stebor>2.0.co;2

Diab, R. D., Thompson, A. M., Mari, K., Ramsay, L., & Coetzee, G. J. R. (2004). Tropospheric ozone climatology over Irene, South Africa, from 1990 to 1994 and 1998 to 2002. *Journal of Geophysical Research*, *109*(D20). https://doi.org/10.1029/2004JD004793

Fleming, Z. L., Doherty, R. M., Von Schneidemesser, E., Malley, C. S., Cooper, O. R., Pinto, J. P., et al. (2018). Tropospheric ozone assessment report: Present-day ozone distribution and trends relevant to human health. *Elementa: Science of the Anthropocene*, *6*, 12. https://doi.org/10.1525/elementa.273

Flemming, J., Benedetti, A., Inness, A., Engelen, R. J., Jones, L., Huijnen, V., et al. (2017). The CAMS interim reanalysis of carbon monoxide, ozone and aerosol for 2003–2015. *Atmospheric Chemistry and Physics*, *17*(3), 1945–1983. https://doi.org/10.5194/acp-17-1945-2017

Flemming, J., Huijnen, V., Arteta, J., Bechtold, P., Beljaars, A., Blechschmidt, A. M., et al. (2015). Tropospheric chemistry in the integrated forecasting system of ECMWF. *Geoscientific Model Development*, *8*(4), 975–1003. https://doi.org/10.5194/gmd-8-975-2015

Flynn, L., Long, C., Wu, X., Evans, R., Beck, C. T., Petropavlovskikh, I., et al. (2014). Performance of the ozone mapping and profiler suite (OMPS) products. *Journal of Geophysical Research: Atmospheres*, *119*(10), 6181–6195. https://doi.org/10.1002/2013JD020467

Fueglistaler, S., Bonazzola, M., Haynes, P. H., & Peter, T. (2005). Stratospheric water vapor predicted from the Lagrangian temperature history of air entering the stratosphere in the tropics. *Journal of Geophysical Research*, *110*(D8), 2004JD005516. https://doi.org/10.1029/2004JD005516

Fueglistaler, S., Dessler, A. E., Dunkerton, T. J., Folkins, I., Fu, Q., & Mote, P. W. (2009). Tropical tropopause layer. *Reviews of Geophysics*, *47*(1), 2008RG000267. https://doi.org/10.1029/2008RG000267

Gaudel, A., Cooper, O. R., Ancellet, G., Barret, B., Boynard, A., Burrows, J. P., et al. (2018). Tropospheric ozone assessment report: Present-day distribution and trends of tropospheric ozone relevant to climate and global atmospheric chemistry model evaluation. *Elementa: Science of the Anthropocene*, *6*, 39. https://doi.org/10.1525/elementa.291

Gelaro, R., McCarty, W., Suárez, M. J., Todling, R., Molod, A., Takacs, L., et al. (2017). The modern-era retrospective analysis for research and applications, version 2 (MERRA-2). *Journal of Climate*, *30*(14), 5419–5454. https://doi.org/10.1175/JCLI-D-16-0758.1

Gettelman, A., & Forster, P. M. D. F. (2002). A climatology of the tropical tropopause layer. *Journal of the Meteorological Society of Japan. Ser. II*, *80*(4B), 911–924. https://doi.org/10.2151/jmsj.80.911

Gettelman, A., Hoor, P., Pan, L. L., Randel, W. J., Hegglin, M. I., & Birner, T. (2011). The extratropical upper troposphere and lower stratosphere. *Reviews of Geophysics*, *49*(3), 2011RG000355. https://doi.org/10.1029/2011RG000355

Global Modeling and Assimilation Office (GMAO). (2015). MERRA-2 inst3_3d_asm_Nv: 3d,3-Hourly, Instantaneous, Model-Level, Assimilation,Assimilated meteorological fields V5.12.4, Greenbelt, MD, USA, Goddard Earth sciences data and information services center (GES DISC) [Dataset]. https://doi.org/10.5067/WWQSXQ8IVFW8

Granier, C., Bessagnet, B., Bond, T., D'Angiola, A., Denier van der Gon, H., Frost, G. J., et al. (2011). Evolution of anthropogenic and biomass burning emissions of air pollutants at global and regional scales during the 1980–2010 period. *Climatic Change*, *109*(1), 163–190. https://doi.org/10.1007/s10584-011-0154-1

Greenslade, J. W., Alexander, S. P., Schofield, R., Fisher, J. A., & Klekociuk, A. K. (2017). Stratospheric ozone intrusion events and their impacts on tropospheric ozone in the Southern Hemisphere. *Atmospheric Chemistry and Physics*, *17*(17), 10269–10290. https://doi.org/10.5194/acp-17-10269-2017

Guenther, A., Karl, T., Harley, P., Wiedinmyer, C., Palmer, P. I., & Geron, C. (2006). Estimates of global terrestrial isoprene emissions using MEGAN (model of emissions of gases and aerosols from nature). *Atmospheric Chemistry and Physics*, *6*(11), 3181–3210. https://doi.org/10.5194/acp-6-3181-2006

Hersbach, H., Bell, B., Berrisford, P., Hirahara, S., Horányi, A., Muñoz-Sabater, J., et al. (2020). The ERA5 global reanalysis. *Quarterly Journal of the Royal Meteorological Society*, *146*(730), 1999–2049. https://doi.org/10.1002/qj.3803

Holton, J. R., Haynes, P. H., McIntyre, M. E., Douglass, A. R., Rood, R. B., & Pfister, L. (1995). Stratosphere-troposphere exchange. *Reviews of Geophysics*, *33*(4), 403–439. https://doi.org/10.1029/95RG02097

Homeyer, C. R., & Bowman, K. P. (2013). Rossby wave breaking and transport between the tropics and extratropics above the subtropical jet. *Journal of the Atmospheric Sciences*, *70*(2), 607–626. https://doi.org/10.1175/JAS-D-12-0198.1

Homeyer, C. R., Pan, L. L., & Barth, M. C. (2014). Transport from convective overshooting of the extratropical tropopause and the role of large-scale lower stratosphere stability. *Journal of Geophysical Research: Atmospheres*, *119*(5), 2220–2240. https://doi.org/10.1002/2013JD020931

Hoor, P., Wernli, H., Hegglin, M. I., & Bönisch, H. (2010). Transport timescales and tracer properties in the extratropical UTLS. *Atmospheric Chemistry and Physics*, *10*(16), 7929–7944. https://doi.org/10.5194/acp-10-7929-2010

Hoskins, B. J., McIntyre, M. E., & Robertson, A. W. (1985). On the use and significance of isentropic potential vorticity maps. *Quarterly Journal of the Royal Meteorological Society*, *111*(470), 877–946. https://doi.org/10.1002/qj.49711147002

Huijnen, V., Miyazaki, K., Flemming, J., Inness, A., Sekiya, T., & Schultz, M. G. (2020). An intercomparison of tropospheric ozone reanalysis products from CAMS, CAMS interim, TCR-1, and TCR-2. *Geoscientific Model Development*, *13*(3), 1513–1544. https://doi.org/10.5194/gmd-13-1513-2020

Hulswar, S., Soni, V. K., Sapate, J. P., More, R. S., & Mahajan, A. S. (2020). Validation of satellite retrieved ozone profiles using in-situ ozonesonde observations over the Indian Antarctic station, Bharati. *Polar Science*, *25*, 100547. https://doi.org/10.1016/j.polar.2020.100547

Hwang, S., Kim, J., & Cho, G. (2007). Observation of secondary ozone peaks near the tropopause over the Korean peninsula associated with stratosphere-troposphere exchange. *Journal of Geophysical Research*, *112*(D16), 2006JD007978. https://doi.org/10.1029/2006JD007978

Inness, A., Ades, M., Agustí-Panareda, A., Barré, J., Benedictow, A., Blechschmidt, A.-M., et al. (2019). The CAMS reanalysis of atmospheric composition. *Atmospheric Chemistry and Physics*, *19*(6), 3515–3556. https://doi.org/10.5194/acp-19-3515-2019

Inness, A., Baier, F., Benedetti, A., Bouarar, I., Chabrillat, S., Clark, H., et al. (2013). The MACC reanalysis: An 8 yr data set of atmospheric composition. *Atmospheric Chemistry and Physics*, *13*(8), 4073–4109. https://doi.org/10.5194/acp-13-4073-2013

Jaross, G., Bhartia, P. K., Chen, G., Kowitt, M., Haken, M., Chen, Z., et al. (2014). OMPS limb profiler instrument performance assessment. *Journal of Geophysical Research: Atmospheres*, *119*(7), 4399–4412. https://doi.org/10.1002/2013JD020482

Kaiser, J. W., Heil, A., Andreae, M. O., Benedetti, A., Chubarova, N., Jones, L., et al. (2012). Biomass burning emissions estimated with a global fire assimilation system based on observed fire radiative power. *Biogeosciences*, *9*(1), 527–554. https://doi.org/10.5194/bg-9-527-2012

Kim, J., Jeong, U., Ahn, M.-H., Kim, J. H., Park, R. J., Lee, H., et al. (2020). New era of air quality monitoring from space: Geostationary environment monitoring spectrometer (GEMS). *Bulletin of the American Meteorological Society*, *101*(1), E1–E22. https://doi.org/10.1175/BAMS-D-18-0013.1

Kim, J., & Koo, J. (2024). ACCLIP: Anmyeon Ozonesonde data. Version 2.0 [Dataset]. *NSF NCAR Earth Observing Laboratory*. https://doi.org/10.26023/39Y4-9RAB-5A0K

Komhyr, W. D. (1969). Electrochemical concentration cells for gas analysis. *Ann. Geoph.*, *25*, 203–210.

Kroon, M., De Haan, J. F., Veefkind, J. P., Froidevaux, L., Wang, R., Kivi, R., & Hakkarainen, J. J. (2011). Validation of operational ozone profiles from the monitoring instrument. *Journal of Geophysical Research*, *116*(D18), D18305. https://doi.org/10.1029/2010jd015100

Leclair De Bellevue, J., Réchou, A., Baray, J. L., Ancellet, G., & Diab, R. D. (2006). Signatures of stratosphere to troposphere transport near deep convective events in the southern subtropics. *Journal of Geophysical Research*, *111*(D24). https://doi.org/10.1029/2005JD006947

Lelieveld, J., & Dentener, F. J. (2000). What controls tropospheric ozone? *Journal of Geophysical Research*, *105*(D3), 3531–3551. https://doi.org/10.1029/1999JD901011

Lemoine, R. (2004). Secondary maxima in ozone profiles. *Atmospheric Chemistry and Physics*, *4*, 1085–1096. https://doi.org/10.5194/acp-4-1085-2004

Levelt, P. F., Van Den Oord, G. H. J., Dobber, M. R., Malkki, A., Visser, H., De Vries, J., et al. (2006). The ozone monitoring instrument. *IEEE Transactions on Geoscience and Remote Sensing*, *44*(5), 1093–1101. https://doi.org/10.1109/TGRS.2006.872333

Liu, J., Rodriguez, J. M., Oman, L. D., Douglass, A. R., Olsen, M. A., & Hu, L. (2020). Stratospheric impact on the Northern Hemisphere winter and spring ozone interannual variability in the troposphere. *Atmospheric Chemistry and Physics*, *20*(11), 6417–6433. https://doi.org/10.5194/acp-20-6417-2020

Manney, G. L., Hegglin, M. I., Daffer, W. H., Santee, M. L., Ray, E. A., Pawson, S., et al. (2011). Jet characterization in the upper troposphere/lower stratosphere (UTLS): Applications to climatology and transport studies. *Atmospheric Chemistry and Physics*, *11*(12), 6115–6137. https://doi.org/10.5194/acp-11-6115-2011

McKenzie, R. L., Aucamp, P. J., Bais, A. F., Björn, L. O., Ilyas, M., & Madronich, S. (2011). Ozone depletion and climate change: Impacts on UV radiation. *Photochemical and Photobiological Sciences*, *10*(2), 182–198. https://doi.org/10.1039/c0pp90034f

McPeters, R., Kroon, M., Labow, G., Brinksma, E., Balis, D., Petropavlovskikh, I., et al. (2008). Validation of the Aura ozone monitoring instrument total column ozone product. *Journal of Geophysical Research*, *113*(D15), 2007JD008802. https://doi.org/10.1029/2007JD008802

McPeters, R. D., & Labow, G. J. (2012). Climatology 2011: An MLS and sonde derived ozone climatology for satellite retrieval algorithms. *Journal of Geophysical Research*, *117*(D10), 2011JD017006. https://doi.org/10.1029/2011JD017006

Miyazaki, K., & Bowman, K. (2017). Evaluation of ACCMIP ozone simulations and ozonesonde sampling biases using a satellite-based multi-constituent chemical reanalysis. *Atmospheric Chemistry and Physics*, *17*(13), 8285–8312. https://doi.org/10.5194/acp-17-8285-2017

Molina, M. J., & Rowland, F. S. (1974). Stratospheric sink for chlorofluoromethanes: Chlorine atom-catalyzed destruction of ozone. *Nature*, *249*(5460), 810–812. https://doi.org/10.1038/249810a0

Molod, A., Takacs, L., Suarez, M., & Bacmeister, J. (2015). Development of the GEOS-5 atmospheric general circulation model: Evolution from MERRA to MERRA2. *Climate and Earth system modeling*. https://doi.org/10.5194/gmdd-7-7575-2014

Monks, P. S., Archibald, A. T., Colette, A., Cooper, O., Coyle, M., Derwent, R., et al. (2015). Tropospheric ozone and its precursors from the urban to the global scale from air quality to short-lived climate forcer. *Atmospheric Chemistry and Physics*, *15*(15), 8889–8973. https://doi.org/10.5194/acp-15-8889-2015

Müller, K., von der Gathen, P., & Rex, M. (2024). Air mass transport to the tropical western Pacific troposphere inferred from ozone and relative humidity balloon observations above Palau. *Atmospheric Chemistry and Physics*, *24*(8), 4693–4716. https://doi.org/10.5194/acp-24-4693-2024

Pan, L. L., Atlas, E. L., Honomichl, S. B., Smith, W. P., Kinnison, D. E., Solomon, S., et al. (2024). East Asian summer monsoon delivers large abundances of very short-lived organic chlorine substances to the lower stratosphere. *Proceedings of the National Academy of Sciences*, *121*(12), e2318716121. https://doi.org/10.1073/pnas.2318716121

Pan, L. L., Atlas, E. L., Newman, P. A., Thornberry, T., Jucks, K. W., Toon, O. B., et al. (2025). The Asian summer monsoon chemical and climate impact project (ACCLIP): An overview. *ESS Open Archive*. https://doi.org/10.22541/essoar.175337658.88281458/v1

Pan, L. L., Kinnison, D., Bian, J., Abalos, M., Randel, W. J., & Bergman, J. W. (2016). Transport of chemical tracers from the boundary layer to stratosphere associated with the dynamics of the Asian summer monsoon. *Journal of Geophysical Research: Atmospheres*, *121*(23). https://doi.org/10.1002/2016JD025616

Pan, L. L., Kinnison, D., Liang, Q., Chin, M., Santee, M. L., Flemming, J., et al. (2022). A multimodel investigation of Asian summer monsoon UTLS transport over the Western Pacific. *Journal of Geophysical Research: Atmospheres*, *127*(24), e2022JD037511. https://doi.org/10.1029/2022jd037511

Park, S., Son, S.-W., Jung, M.-I., Park, J., & Park, S. S. (2020). Evaluation of tropospheric ozone reanalyses with independent ozonesonde observations in East Asia. *Geoscience Letters*, *7*(1), 12. https://doi.org/10.1186/s40562-020-00161-9

Park, S. S., Kim, J., Cho, H. K., Lee, H., Lee, Y., & Miyagawa, K. (2012). Sudden increase in the total ozone density due to secondary ozone peaks and its effect on total ozone trends over Korea. *Atmospheric Environment*, *47*, 226–235. https://doi.org/10.1016/j.atmosenv.2011.11.011

Portafaix, T., Morel, B., Bencherif, H., Baldy, S., Godin-Beekmann, S., & Hauchecorne, A. (2003). Fine-scale study of a thick stratospheric ozone lamina at the edge of the southern subtropical barrier. *Journal of Geophysical Research*, *108*(D6). https://doi.org/10.1029/2002JD002741

Postel, G. A., & Hitchman, M. H. (1999). A climatology of rossby wave breaking along the subtropical tropopause. *Journal of the Atmospheric Sciences*, *56*(3), 359–373. https://doi.org/10.1175/1520-0469(1999)056<0359:acorwb>2.0.co;2

Price, J. D., & Vaughan, G. (1993). The potential for stratosphere-troposphere exchange in cut-off-low systems. *Quarterly Journal of the Royal Meteorological Society*, *119*(510), 343–365. https://doi.org/10.1002/qj.49711951007

Randel, W. J., & Wu, F. (2007). A stratospheric ozone profile data set for 1979–2005: Variability, trends, and comparisons with column ozone data. *Journal of Geophysical Research*, *112*(D6), 2006JD007339. https://doi.org/10.1029/2006JD007339

Reid, S. J., & Vaughan, G. (1991). Lamination in ozone profiles in the lower stratosphere. *Quarterly Journal of the Royal Meteorological Society*, *117*(500), 825–844. https://doi.org/10.1002/qj.49711750009

Riese, M., Ploeger, F., Rap, A., Vogel, B., Konopka, P., Dameris, M., & Forster, P. (2012). Impact of uncertainties in atmospheric mixing on simulated UTLS composition and related radiative effects. *Journal of Geophysical Research*, *117*(D16), 2012JD017751. https://doi.org/10.1029/2012JD017751

Rodgers, C. D., & Connor, B. J. (2003). Intercomparison of remote sounding instruments. *Journal of Geophysical Research*, *108*(D3), 2002JD002299. https://doi.org/10.1029/2002JD002299

Ryu, Y.-H., & Min, S.-K. (2021). Long-term evaluation of atmospheric composition reanalyses from CAMS, TCR-2, and MERRA-2 over South Korea: Insights into applications, implications, and limitations. *Atmospheric Environment*, *246*, 118062. https://doi.org/10.1016/j.atmosenv.2020.118062

Sekiya, T., Emili, E., Miyazaki, K., Inness, A., Qu, Z., Pierce, R. B., et al. (2025). Assessing the relative impacts of satellite ozone and its precursor observations to improve global tropospheric ozone analysis using multiple chemical reanalysis systems. *Atmospheric Chemistry and Physics*, *25*(4), 2243–2268. https://doi.org/10.5194/acp-25-2243-2025

Shangguan, M., Wang, W., & Jin, S. (2019). Variability of temperature and ozone in the upper troposphere and lower stratosphere from multi-satellite observations and reanalysis data. *Atmospheric Chemistry and Physics*, *19*(10), 6659–6679. https://doi.org/10.5194/acp-19-6659-2019

Shin, D., Song, S., Ryoo, S.-B., & Lee, S.-S. (2020). Variations in ozone concentration over the mid-latitude region revealed by ozonesonde observations in Pohang, South Korea. *Atmosphere*, *11*(7), 746. https://doi.org/10.3390/atmos11070746

Škerlak, B., Sprenger, M., & Wernli, H. (2014). A global climatology of stratosphere–troposphere exchange using the ERA-Interim data set from 1979 to 2011. *Atmospheric Chemistry and Physics*, *14*(2), 913–937. https://doi.org/10.5194/acp-14-913-2014

Smit, H. G., Straeter, W., Johnson, B. J., Oltmans, S. J., Davies, J., Tarasick, D. W., et al. (2007). Assessment of the performance of ECC-ozonesondes under quasi-flight conditions in the environmental simulation chamber: Insights from the Juelich ozone Sonde intercomparison experiment (JOSIE). *Journal of Geophysical Research*, *112*(D19). https://doi.org/10.1029/2006jd007308

Smit, H. G. J., & ASOPOS Panel. (2014). *Quality assurance and quality control for ozonesonde measurements in GAW*. GAW Report 201. World Meteorological Organization.

Smit, H. G. J., & Thompson, A. M. (2021). *Ozonesonde measurement principles and best operational practices: Asopos 2.0*. GAW Report No. 268. World Meteorological Organization.

Solomon, S. (1999). Stratospheric ozone depletion: A review of concepts and history. *Reviews of Geophysics*, *37*(3), 275–316. https://doi.org/10.1029/1999RG900008

Sprenger, M., Croci Maspoli, M., & Wernli, H. (2003). Tropopause folds and cross-tropopause exchange: A global investigation based upon ECMWF analyses for the time period March 2000 to February 2001. *Journal of Geophysical Research*, *108*(D12), 2002JD002587. https://doi.org/10.1029/2002JD002587

Stajner, I., Wargan, K., Pawson, S., Hayashi, H., Chang, L. P., Hudman, R. C., et al. (2008). Assimilated ozone from EOS-Aura: Evaluation of the tropopause region and tropospheric columns. *Journal of Geophysical Research*, *113*(D16). https://doi.org/10.1029/2007jd008863

Stauffer, R. M., Thompson, A. M., Kollonige, D. E., Komala, N., Al-Ghazali, H. K., Risdianto, D. Y., et al. (2024). Dynamical drivers of free-tropospheric ozone increases over equatorial southeast Asia. *Atmospheric Chemistry and Physics*, *24*(9), 5221–5234. https://doi.org/10.5194/acp-24-5221-2024

Stauffer, R. M., Thompson, A. M., Kollonige, D. E., Tarasick, D. W., Van Malderen, R., Smit, H. G. J., et al. (2022). An examination of the recent stability of ozonesonde global network data. *Earth and Space Science*, *9*(10), e2022EA002459. https://doi.org/10.1029/2022EA002459

Stauffer, R. M., Thompson, A. M., & Witte, J. C. (2018). Characterizing global ozonesonde profile variability from surface to the UT/LS with a clustering technique and MERRA-2 reanalysis. *Journal of Geophysical Research: Atmospheres*, *123*(11), 6213–6229. https://doi.org/10.1029/2018JD028465

Stohl, A., Bonasoni, P., Cristofanelli, P., Collins, W., Feichter, J., Frank, A., et al. (2003). Stratosphere-troposphere exchange: A review, and what we have learned from STACCATO. *Journal of Geophysical Research*, *108*(D12), 2002JD002490. https://doi.org/10.1029/2002JD002490

Stohl, A., Wernli, H., James, P., Bourqui, M., Forster, C., Liniger, M. A., et al. (2003). A new perspective of stratosphere–troposphere exchange. *Bulletin of the American Meteorological Society*, *84*(11), 1565–1574. https://doi.org/10.1175/BAMS-84-11-1565

Tao, M., Pan, L. L., Konopka, P., Honomichl, S. B., Kinnison, D. E., & Apel, E. C. (2018). A Lagrangian model diagnosis of stratospheric contributions to tropical midtropospheric air. *Journal of Geophysical Research: Atmospheres*, *123*(17), 9764–9785. https://doi.org/10.1029/2018jd028696

Tarasick, D. W., Carey-Smith, T. K., Hocking, W. K., Moeini, O., He, H., Liu, J., et al. (2019). Quantifying stratosphere-troposphere transport of ozone using balloon-borne ozonesondes, radar windprofilers and trajectory models. *Atmospheric Environment*, *198*, 496–509. https://doi.org/10.1016/j.atmosenv.2018.10.040

Tarasick, D. W., Smit, H. G. J., Thompson, A. M., Morris, G. A., Witte, J. C., Davies, J., et al. (2021). Improving ECC ozonesonde data quality: Assessment of current methods and outstanding issues. *Earth and Space Science*, *8*(3), e2019EA000914. https://doi.org/10.1029/2019EA000914

Thompson, A. M., Smit, H. G. J., Witte, J. C., Stauffer, R. M., Johnson, B. J., Morris, G., et al. (2019). Ozonesonde quality assurance: The JOSIE–SHADOZ (2017) experience. *Bulletin of the American Meteorological Society*, *100*(1), 155–171. https://doi.org/10.1175/BAMS-D-17-0311.1

Thompson, A. M., Stone, J. B., Witte, J. C., Miller, S. K., Oltmans, S. J., Kucsera, T. L., et al. (2007b). Intercontinental chemical transport experiment ozonesonde network study (IONS) 2004: 2. Tropospheric ozone budgets and variability over northeastern North America. *Journal of Geophysical Research*, *112*(D12), 2006JD007670. https://doi.org/10.1029/2006JD007670

Thompson, A. M., Stone, J. B., Witte, J. C., Miller, S. K., Pierce, R. B., Chatfield, R. B., et al. (2007a). Intercontinental chemical transport experiment ozonesonde network study (IONS) 2004: 1. Summertime upper troposphere/lower stratosphere ozone over northeastern North America. *Journal of Geophysical Research*, *112*(D12), 2006JD007441. https://doi.org/10.1029/2006JD007441

Thompson, A. M., Witte, J. C., Smit, H. G. J., Oltmans, S. J., Johnson, B. J., Kirchhoff, V. W. J. H., & Schmidlin, F. J. (2007). Southern hemisphere additional ozonesondes (SHADOZ) 1998–2004 tropical ozone climatology: 3. Instrumentation, station-to-station variability, and evaluation with simulated flight profiles. *Journal of Geophysical Research*, *112*(D3), 2005JD007042. https://doi.org/10.1029/2005JD007042

Thompson, A. M., Witte, J. C., Sterling, C., Jordan, A., Johnson, B. J., Oltmans, S. J., et al. (2017). First reprocessing of southern hemisphere additional ozonesondes (SHADOZ) ozone profiles (1998–2016): 2. Comparisons with satellites and ground-based instruments. *Journal of Geophysical Research: Atmospheres*, *122*(23). https://doi.org/10.1002/2017JD027406

Thompson, A. M., Yorks, J. E., Miller, S. K., Witte, J. C., Dougherty, K. M., Morris, G. A., et al. (2008). Tropospheric ozone sources and wave activity over Mexico City and Houston during MILAGRO/intercontinental transport experiment (INTEX-B) ozonesonde network study, 2006 (IONS-06). *Atmospheric Chemistry and Physics*, *8*(17), 5113–5125. https://doi.org/10.5194/acp-8-5113-2008

Thorncroft, C. D., Hoskins, B. J., & McIntyre, M. E. (1993). Two paradigms of baroclinic-wave life-cycle behaviour. *Quarterly Journal of the Royal Meteorological Society*, *119*(509), 17–55. https://doi.org/10.1002/qj.49711950903

Thouret, V., Cammas, J. P., Sauvage, B., Athier, G., Zbinden, R., Nédélec, P., et al. (2006). Tropopause referenced ozone climatology and inter-annual variability (1994–2003) from the MOZAIC programme. *Atmospheric Chemistry and Physics*, *6*(4), 1033–1051. https://doi.org/10.5194/acp-6-1033-2006

Trickl, T., Cooper, O. R., Eisele, H., James, P., Mücke, R., & Stohl, A. (2003). Intercontinental transport and its influence on the ozone concentrations over central Europe: Three case studies. *Journal of Geophysical Research*, *108*(D12), 2002JD002735. https://doi.org/10.1029/2002JD002735

Trickl, T., Feldmann, H., Kanter, H. J., Scheel, H. E., Sprenger, M., Stohl, A., & Wernli, H. (2010). Forecasted deep stratospheric intrusions over central Europe: Case studies and climatologies. *Atmospheric Chemistry and Physics*, *10*(2), 499–524. https://doi.org/10.5194/acp-10-499-2010

Verhoelst, T., Granville, J., Hendrick, F., Köhler, U., Lerot, C., Pommereau, J.-P., et al. (2015). Metrology of ground-based satellite validation: Co-location mismatch and smoothing issues of total ozone comparisons. *Atmospheric Measurement Techniques*, *8*(12), 5039–5062. https://doi.org/10.5194/amt-8-5039-2015

Wagner, A., Bennouna, Y., Blechschmidt, A.-M., Brasseur, G., Chabrillat, S., Christophe, Y., et al. (2021). Comprehensive evaluation of the copernicus atmosphere monitoring service (CAMS) reanalysis against independent observations. *Elementa: Science of the Anthropocene*, *9*(1), 00171. https://doi.org/10.1525/elementa.2020.00171

Wagner, A., Schulz, M., Christophe, Y., Ramonet, M., Eskes, H. J., Basart, S., et al. (2019). Validation report of the CAMS near-real-time global atmospheric composition service: Period September – November 2019. https://doi.org/10.24380/XZKK-BZ05

Wargan, K., Labow, G., Frith, S., Pawson, S., Livesey, N., & Partyka, G. (2017). Evaluation of the ozone fields in NASA's MERRA-2 reanalysis. *Journal of Climate*, *30*(8), 2961–2988. https://doi.org/10.1175/jcli-d-16-0699.1

Wargan, K., Pawson, S., Olsen, M. A., Witte, J. C., Douglass, A. R., Ziemke, J. R., et al. (2015). The global structure of upper troposphere-lower stratosphere ozone in GEOS-5: A multiyear assimilation of EOS Aura data. *Journal of Geophysical Research: Atmospheres*, *120*(5), 2013–2036. https://doi.org/10.1002/2014jd022493

Witte, J. C., Thompson, A. M., Smit, H. G. J., Fujiwara, M., Posny, F., Coetzee, G. J. R., et al. (2017). First reprocessing of Southern Hemisphere ADditional OZonesondes (SHADOZ) profile records (1998–2015): 1. Methodology and evaluation. *Journal of Geophysical Research: Atmospheres*, *122*(12), 6611–6636. https://doi.org/10.1002/2016JD026403

World Meteorological Organization. (1957). Meteorology—A three dimensional science: Second session of the commission for aerology. *World Meteorological Organization Bulletin*, *IV*(4), 134–138.

Xu, J., Zhang, Z., Rao, L., Wang, Y., Letu, H., Shi, C., et al. (2024). Remote sensing of tropospheric ozone from space: Progress and challenges. *Journal of Remote Sensing*, *4*, 0178. https://doi.org/10.34133/remotesensing.0178

Yorks, J. E., Thompson, A. M., Joseph, E., & Miller, S. K. (2009). The variability of free tropospheric ozone over Beltsville, Maryland (39N, 77W) in the summers 2004–2007. *Atmospheric Environment*, *43*(11), 1827–1838. https://doi.org/10.1016/j.atmosenv.2008.12.049

Zbinden, R. M., Thouret, V., Ricaud, P., Carminati, F., Cammas, J.-P., & Nédélec, P. (2013). Climatology of pure tropospheric profiles and column contents of ozone and carbon monoxide using MOZAIC in the mid-northern latitudes (24° N to 50° N) from 1994 to 2009. *Atmospheric Chemistry and Physics*, *13*(24), 12363–12388. https://doi.org/10.5194/acp-13-12363-2013

Zhang, Y., Huang, Q., Guo, K., Wang, M., Liao, H., Chou, Y., & He, X. (2024). Tropopause folds over the Tibetan Plateau and their impact on water vapor in the upper troposphere-lower stratosphere. *Climate Dynamics*, *62*(2), 1423–1437. https://doi.org/10.1007/s00382-023-06978-2

Ziemke, J. R., Chandra, S., Labow, G. J., Bhartia, P. K., Froidevaux, L., & Witte, J. C. (2011). A global climatology of tropospheric and stratospheric ozone derived from Aura OMI and MLS measurements. *Atmospheric Chemistry and Physics*, *11*(17), 9237–9251. https://doi.org/10.5194/acp-11-9237-2011